Materials Science & Engineering A 805 (2021) 140594

Contents lists available at ScienceDirect

Materials Science & Engineering A

journal homepage: http://www.elsevier.com/locate/msea

Repeatability of the fatigue performance of additively manufactured A357.0 under different thermal treatment conditions

S. Defanti, E. Bassoli *

Department of Engineering "Enzo Ferrari" (DIEF), University of Modena and Reggio Emilia, 41125, Modena, MO, Italy

ARTICLE INFO

Keywords:
A357.0
Laser-based powder bed fusion
Additive manufacturing
Thermal treatment
Fatigue

ABSTRACT

A357.0 parts were produced by laser-based powder bed fusion. An in-situ annealing strategy was applied by pre-heating the build platform, in order to relieve residual stresses and reduce anisotropic effects upon processing. The mean value and standard deviation for the fatigue strength at the given life time of 1×10^7 cycles were determined according to the staircase method, before and after T6 heat treatment. Samples parallel to the build platform and parallel to the growth direction were analysed separately and compared. The fatigue behaviour was substantially insensitive to post-processing heat treatment, since fracture initiation was governed by sub-surface lack-of-fusion defects that remained unchanged in the T6 conditions. The heat treatment caused an increase in porosity, yet without significant detriment to the fatigue resistance. The build orientation was not found to affect the average value of the fatigue strength, but it caused variations of the repeatability.

1. Introduction

The present contribution is specifically addressed to investigate the effect of thermal treatment on the fatigue resistance of aluminium alloy parts produced by means of laser-based powder bed fusion (L-PBF).

Thermal effects in L-PBF are quite different from those conventionally encountered in casting. Generally speaking, laser-based processing causes relevant frozen stresses as a consequence of the steep thermal gradients that are established between the melt pool and the surrounding material, with subsequent cooling rates as high as 10^6 K/s [1]. During solidification of each molten track, as well as during cooling-down of the last-built layer, shrinkage is hindered by the underlying colder material. As a consequence, tensile stresses get frozen into the material [2,3]. When the part is cut from the build platform, residual stresses in the built part are greatly relaxed through shrinkage and deformation [4]. However, as-built components are usually affected by tensile stresses in the upper and lower layers, and by compressive stresses in the intermediate zone [2,5]. A further complexity derives from the repeated thermal cycles that the material experiences due to the partial remelting of each layer when the subsequent slice is irradiated [1,6].

The combined effect of the described phenomena turns into a high risk of part distortion, leading to loss of dimensional tolerances in the best case, or even to job failure if the part rises out of the powder bed and is hit by the recoater, in the worst case.

Two different strategies have been proposed to limit the intensity of residual stresses, namely (i) in-situ methods and (ii) post-process methods [7]. A common in-situ method consists in heating up the build platform before and during the build, so that a reduced cooling rate is achieved as compared to the unheated counterpart and, at the same time, a stress relieving effect is attained while processing, which also reduces the anisotropy of the as-built part [1]. Buchbinder et al. [8] studied the production of AlSi10Mg twin cantilevers and they proved a relevant reduction of distortion as a consequence of substrate pre-heating to 200 °C. However, Brandl et al. [9] pointed out that the platform pre-heating did not change the mean fatigue strength of their AlSi10Mg L-PBF parts, but helped to reduce the data scattering.

As an alternative or additional treatment, ex-situ post-processing is also feasible [7,10,11]. For example, shot-peening treatment allowed to induce a smooth and controlled superficial compression state in AlSi10Mg parts produced via L-PBF with and without supports [12,13]. Otherwise, a stress relief thermal treatment can be performed after printing [9].

The effect of baseplate pre-heating and post-processing thermal treatment on aluminium-based parts produced via L-PBF is the object of intensive research [1]. In particular, A357.0 (Al–7Si–Mg alloy [14]) is a casting aluminium alloy that, if processed by conventional techniques, is mainly used in the T6 condition [15]. The T6 heat treatment is intended

* Corresponding author.
E-mail address: elena.bassoli@unimore.it (E. Bassoli).

https://doi.org/10.1016/j.msea.2020.140594
Received 25 September 2020; Received in revised form 23 November 2020; Accepted 23 November 2020
Available online 27 November 2020

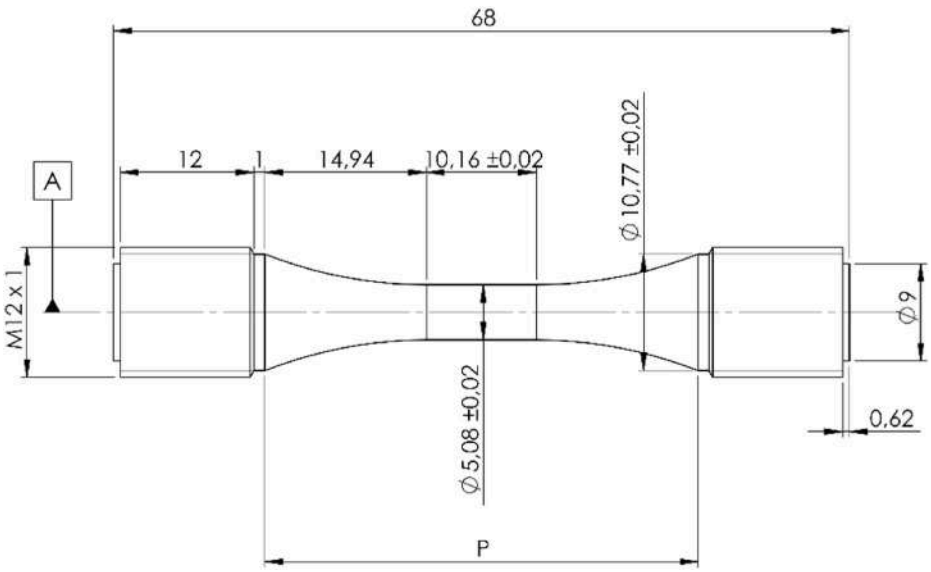

Fig. 1. Geometry and dimensions for fatigue test pieces; dimensions are in millimeters [UNI EN 3987:2010].

to increase the ultimate tensile strength, usually at the expenses of fracture strain. While the consequences of the T6 heat treatment on cast A357.0 parts have been extensively studied in the literature [16], the effects on AM workpieces is still controversial due to their out-of-equilibrium microstructure and complicated thermal history [17–19]. Trevisan et al. [19] proved that A357.0 parts produced by L-PBF (platform pre-heating at 100 °C) in the as-built condition are stronger not only as compared to the stress-relieved state, but also to the T6 condition. Hardness and tensile strength sensibly decreased after stress relieving as a consequence of grain coarsening and of migration of silicon from supersaturated α-Al. Then, precipitation hardening through the formation of stable Mg_2Si particles leads to a partial recovery, but the as-built performance remains unequalled [15]. Even the effect of baseplate heating is still open to discussion for A357.0 components. For example, Rao et al. [20] observed that A357.0 parts built with a platform temperature of 200 °C had lower yield and ultimate tensile strength than the counterparts processed at 35 °C, probably as a consequence of over-aging phenomena. Increasing evidence suggests that thermal treatments for AM parts should be developed on purpose, since the mere replication of conditions that proved successful for cast parts can lead to unexpected results [21,22].

Furthermore, the T6 heat treatment is known to increase the porosity percentage in A357 parts manufactured by L-PBF. During the building process, even with optimized laser parameters, small gas pores are generated due to hydrogen release [23], however, these pores are very small and the part density is still higher than 99.4% [22]. After a Solution Heat Treatment (SHT) as in the T6, the small pores characterizing the as-built condition enlarge, leading to a decrease in the density to 98.4% or less (depending on the temperature and time of the SHT) [23]. The same behaviour is confirmed by Pereira et al. [24] who also observe a decrease in HV1 hardness.

The present research considered samples in the “as-built” condition (i.e. aged in-situ by pre-heating the base plate at 165 °C, but not subjected to any ex-situ heat treatment) and in the “heat-treated” state (i.e. aged in-situ and also subjected to ex-situ T6 heat treatment). Samples manufactured under the same processing conditions were directly compared in order to verify the effect of post-processing heat treatment on fatigue resistance.

2. Materials and methods

All the specimens for the fatigue tests were produced on an EOS M400-1 (EOS GmbH Electro Optical Systems, Krailling/Munich, Germany) L-PBF machine. The parameter set was EOSM400 AlF357 060 V1 (AlF357_060_FlexM400_100), with a layer thickness of 60 μm and a specific energy of 34.7 J/mm^3. The build platform was pre-heated to a temperature of 165 °C that, according to the literature, should be high enough for an in-situ stress-relief of aluminium alloys [8]. The geometry of the samples for the fatigue tests complied with the specifications of UNI EN 3987:2010 [25]. The corresponding dimensions, expressed in millimeters, are specified in Fig. 1. In order to ascertain the potential anisotropy of finished parts with baseplate pre-heating before and after T6 thermal treatment, half of the parts were built parallel to the baseplate (named “XY” parts) and half parallel to the building direction (“Z” parts).

Table 1
Residual porosity for each group of samples as determined via image analysis and by the Archimedes method.

Sample	Porosity, image [%]	Porosity, Archimedes [%]
XY-AB	0.15	0.19
Z-AB	0.30	0.15
XY-T6	0.75	1.27
Z-T6	0.83	1.01

Specimens were built by L-PBF as cylinders, machined to the dimensions in Fig. 1 and polished to an average areal surface roughness (S_a) of 0.2 μm. Then, half of the workpieces of each type (“XY” and “Z”) were tested directly (later on, labelled as “AB”), half after a T6 heat treatment (labelled “T6”).

The axial fatigue tests were performed on a Rumul Mikrotron (RUMUL, Russenberger Prüfmaschinen AG, Neuhausen am Rheinfall, Switzerland) testing machine. The staircase method, as described in ISO 12107:2012 [26], was applied to obtain the mean value of the fatigue strength and an estimate of the standard deviation, useful to estimate the data scattering that is typical for the fatigue resistance of AM parts [27]. Mean value and standard deviation for the fatigue strength were calculated for different levels of probability of failure (P (%) = 50% and P (%) = 10%) at a confidence level of 90%, corresponding to general engineering applications. A loading frequency of 79 Hz and a stress ratio $R = \sigma_{min}/\sigma_{max} = 0.01$ were applied according to ASTM E466-15 [28]. The stress step was set to 10 MPa and the run-out limit was fixed to 1×10^7 cycles.

The fractured surfaces were observed with a scanning electron

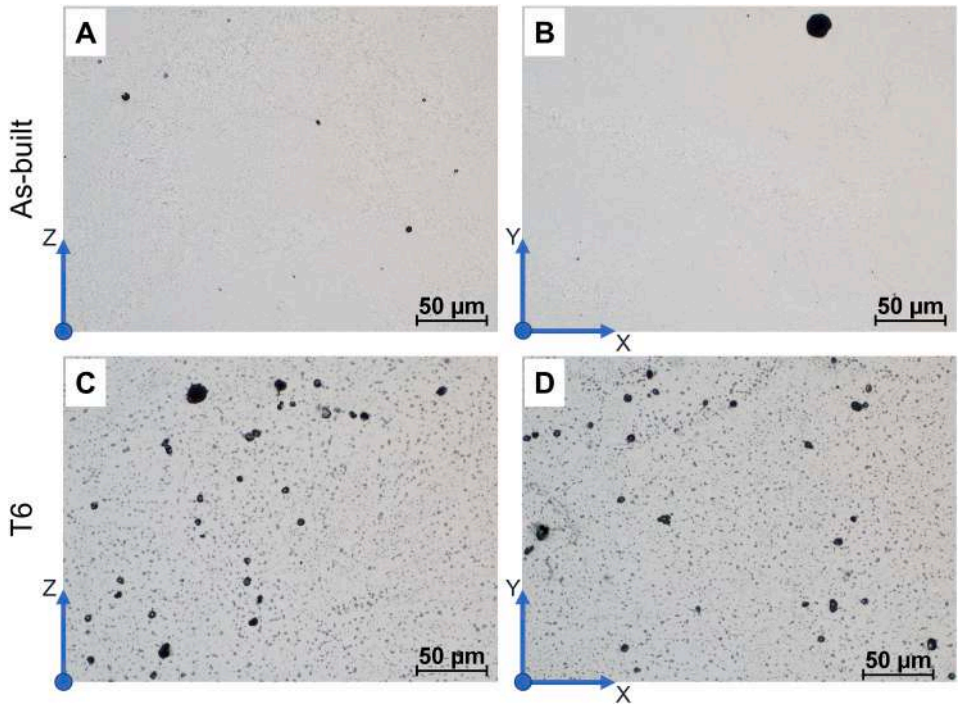

Fig. 2. OM images of the polished cross sections of the samples XY-AB (A), Z-AB (B), XY-T6 (C), and Z-T6 (D).

microscope, SEM (ESEM, Quanta-200, FEI Company, The Netherland). For each group of samples, as listed in Table 1, two specimens were examined, in particular: (i) the sample that broke after the highest number of cycles under the first peak stress level above the average fatigue life calculated for the corresponding group (hereafter: "average samples"); (ii) the specimen with the shortest life under the lowest peak stress level tested for the corresponding group (hereafter: "early broken samples").

Moreover, one sample of each group was sectioned and polished in order to investigate porosity and microstructure by using an optical microscope, OM (Eclipse LV150 N, Nikon, Tokyo, Japan).

Residual porosity before and after T6 treatment was measured by OM image analysis. Three 50x images were considered for each sample. Porosity (P), which correlates with the experimental density (ρ_{ex}) through the equation

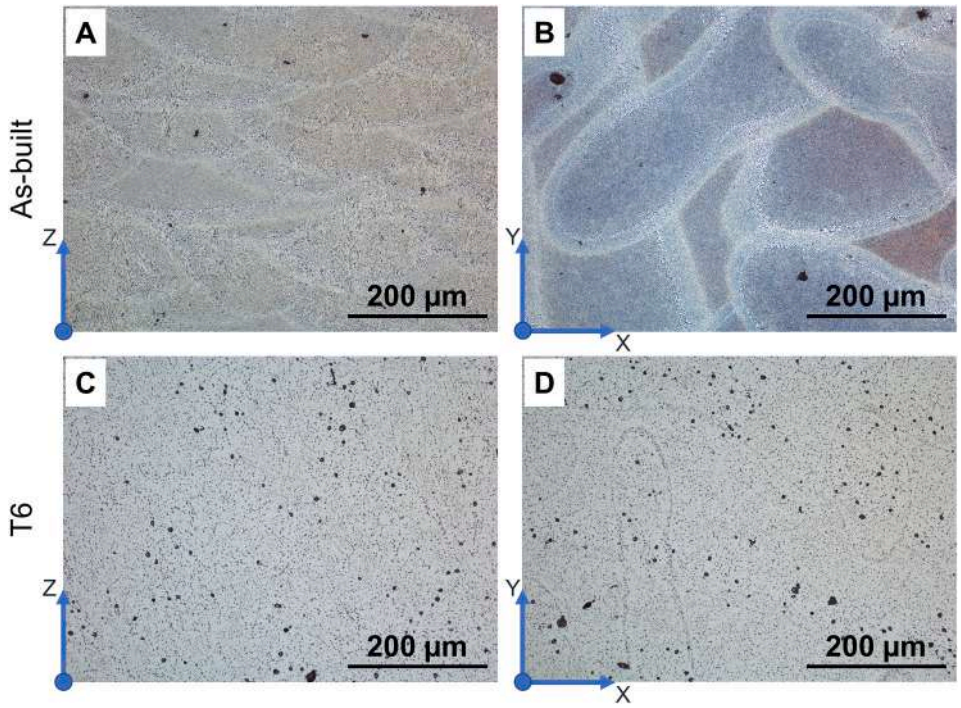

Fig. 3. OM images of the etched cross sections of the samples: XZ section of an AB sample (A), XY section of an AB sample (B), XZ section of a T6 sample (C), and XY section of a T6 sample (D).

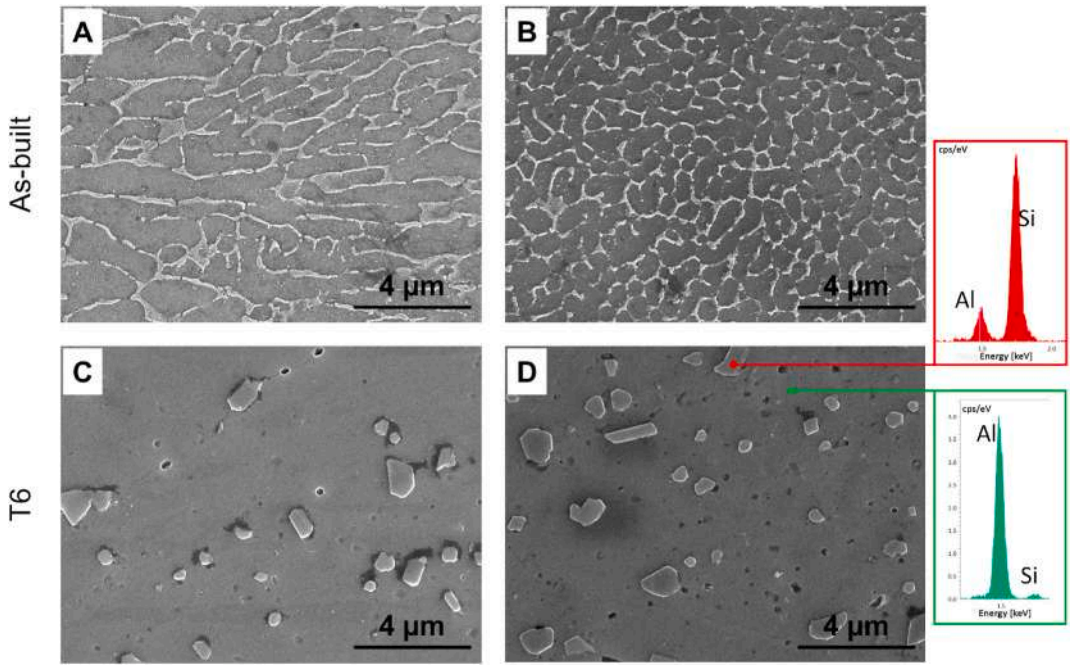

Fig. 4. FEG-SEM images of the polished cross sections of the samples XY-AB (A), Z-AB (B), XY-T6 (C), and Z-T6 (D). In (D), X-EDS spectra collected on the precipitates and on the surrounding matrix.

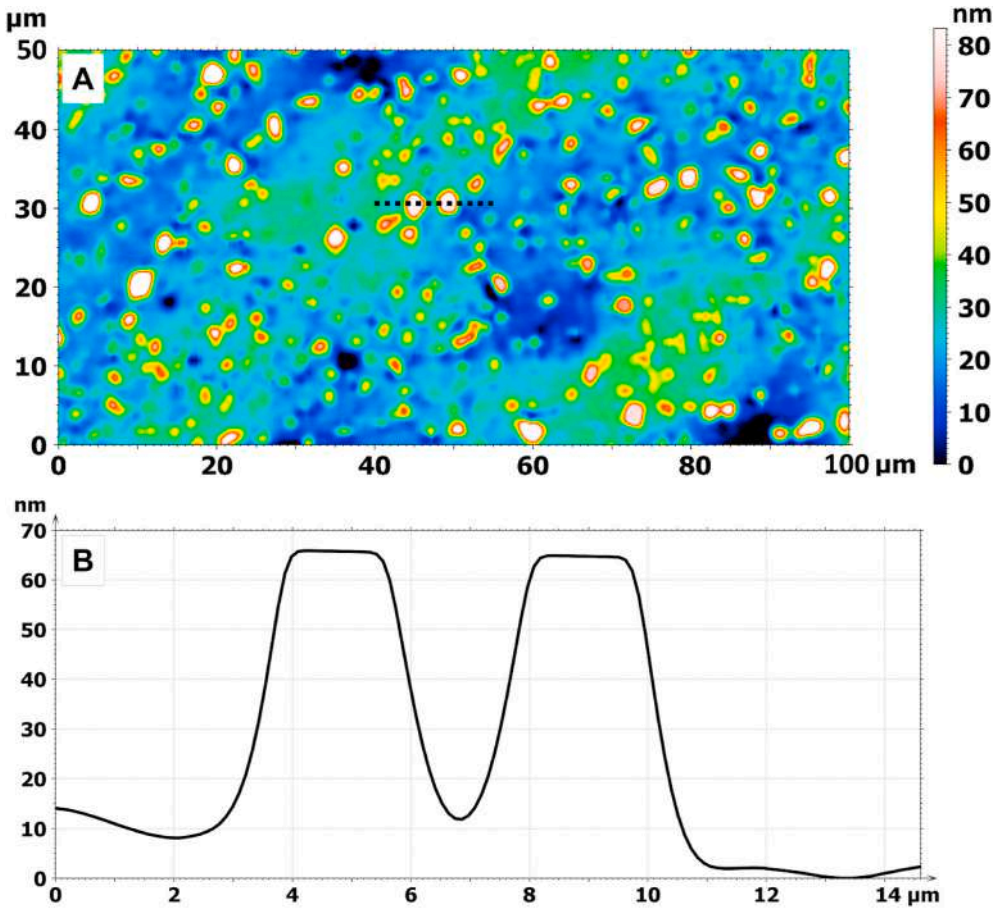

Fig. 5. Height map (A) and line profile (B) acquired on the polished and etched cross section of a sample of the XY-T6 type. The line profile in (B) corresponds to the dotted line in (A).

$$P = \left(1 - \frac{\rho_{ex}}{\rho_{th}}\right) \cdot 100 \quad (1)$$

where ρ_{th} is the theoretical density of A357.0 [29], was also determined by means of the Archimedes method in deionised water (correction of buoyancies was applied).

Hardness was measured using the Brinell Hardness scale HBW 2.5/62.5 according to ISO 6506 [30]. Four indentations were performed on a sample of each group with a ERNST NR3DR hardness tester.

The polished cross sections were also etched with the Dix-Keller reactant (HF 2% vol, HCl 1.5% vol, HNO3 2.5% vol; water bal.) and observed by a Nova NanoSEM 450 FEG-SEM (FEI, ThermoFisher Scientific, Eindhoven, The Netherland) in immersion lens mode, equipped with X-EDS Bruker QUANTAX-200 microanalysis. The polished and etched cross section of a sample of the XY-T6 type was also analysed using the Nikon LV 150 Confovis Microscope instrument. A surface map was acquired on a 100 μm × 50 μm area and line profiles were scanned on specific surface features.

3. Results and discussion

Table 1 summarizes the results obtained for porosity by image analysis and by the Archimedes method. Representative OM images used to measure porosity are shown in Fig. 2.

According to Spierings et al. [31], in principle the porosity values determined through the Archimedes method are expected to be more reliable than those based on image analysis, since all the volume of the sample is taken into account, and not just some single cross sectional areas. On the other hand, the preliminary machining operation may cause the opening of sub-superficial pores [22], thus influencing the results achieved with the Archimedes method [31]. Nonetheless, it is interesting to note that, in the present case, both experimental approaches gave comparable results and confirmed that AB samples were almost fully dense (Fig. 2A and B), as all the corresponding porosity values ranged between 0.15% and 0.30% independently of the building orientation. After T6 treatment (Fig. 2C and D), the porosity percentage significantly increased to around 1%, as a consequence of heat-induced pore formation [21].

Brinell hardness of the AB samples resulted in an average value of 121.1 (SD 1.7), while a slightly lower value of 110.2 (SD 2.5) was obtained on T6 specimens.

The microstructural features can be observed in the OM images in Fig. 3 and in the FEG-SEM images in Fig. 4, showing etched sections parallel to the XY or Z directions for the AB and T6 specimens. Fig. 4A and C shows the cross section of XY samples, which means they show the cross section parallel to the growth (Z) direction before and after T6 treatment, respectively. Analogously, Fig. 4B and D displays the cross section of Z samples, which means they display the cross section parallel to the baseplate (and normal to the growth (Z) direction) before and after T6 treatment. . The melt pools are all partly inter-connected, which ensures perfect bonding between adjacent layers (Fig. 3A). On the contrary, long laser scan tracks can be distinguished in the micrographs parallel to the build platform in Fig. 3B. Overlapped scan tracks are differently oriented as a result of the specific scanning strategy used to build the samples [20]. As already described by Aboulkhair et al. [32], the melt pools and the overlapped tracks are clearly visible for the AB samples, whereas these structures get almost completely smoothed out during the heat treatment, while porosity develops along the track boundaries. (Fig. 3C and D). In addition, as a consequence of the T6 treatment, silicon diffuses and precipitates to form spheroidal Mg_2Si particles in the aluminium matrix. The relative chemical composition of the matrix and of the precipitates can be evaluated in Fig. 4D, showing the X-EDS spectra collected on the two areas. This progressive transformation results therefore into a more homogenous microstructure, because the original L-PBF features are overshadowed by the heat-induced spatial redistribution and rearrangement of the constituent elements [9,32]. Additionally, Fig. 3C and D prove the increased porosity as a consequence of the T6 treatment [21], thus validating the results in Table 1. Fig. 5Ashows the height map acquired on the polished and etched cross section of a XY-T6 sample. Mg_2Si precipitates protrude out of the flat aluminum matrix, as highlighted by the linear profile in Fig. 5B. The morphology has close similarity with aluminium-silicon alloy cylinder liner material, which includes a soft aluminium matrix inlaid with hard silicon particles. In fact, for this specific application, the ideal surface is characterized by hard silicon particles, which should bear the load, and a slightly concave aluminium base, which should store the oil to promote lubrication [33].

Table 2
Fatigue strength at the given run out limit of 1×10^7 cycles: mean value for different levels of probability of failure (P (%) = 50% and P (%) = 10%, confidence level 90%) and standard deviation.

Sample	Fatigue strength [MPa] (confidence level = 90%)		
	P (%) = 50%	P (%) = 10%	Std Dev
XY-AB	135	123	5
Z-AB	122	98	10
XY-T6	126	110	7
Z-T6	124	96	12

Table 2 reports the outcomes of the fatigue tests. Based on the staircase method as prescribed by ISO 12107:2012 [26], the fatigue strength at the given life time of 1×10^7 cycles was expressed as the mean value ± standard deviation, for different levels of probability of failure (P (%) = 50% and P (%) = 10%), at a confidence level of 90%.

The baseplate pre-heating temperature that was applied in the present research was chosen according to the available literature in order to reach an optimal compromise between in-situ stress relief and need to avoid microstructural coarsening. In fact, Buchbinder et al. [8] investigated the residual stress-induced distortion of AlSi10Mg parts during L-PBF as a function of the baseplate pre-heating temperature and demonstrated that a relevant decrease in distortion could be detected starting from 150 °C and distortion became totally negligible at a pre-heating temperature of 250 °C [8]. However, as a consequence of pre-heating, the solidification rate became slower and, starting from a temperature of 200 °C, a significant coarsening occurred in terms of dendrite and grain size. The mechanical behaviour became more ductile, at the expenses of hardness and strength [34]. Aversa et al. [1] focused their attention on A357.0 parts built by L-PBF with different baseplate temperatures of 100, 140, 170 and 190 °C. Higher baseplate temperatures enabled the precipitation of Mg_2Si during the L-PBF process, thus inducing an in-situ aging effect. Nevertheless, when the baseplate temperature was increased to 190 °C, the tensile strength decreased back to a value comparable to that of the samples built at 100 °C as a consequence of over-ageing. Then, a post-process heat treatment was performed at 170 °C and the effect on hardness was determined as a function of heating time. The hardness of the samples built at 100 °C and 140 °C could be increased for treatments up to as long as 3 h at 170 °C. For the samples produced at 170 °C and 190 °C, instead, the heat treatment at 170 °C had negative consequences independently of its duration due to the increased over-aging effect [1].

A similar tendency to microstructural coarsening was observed also during post-processing heat treatment by Prashanth et al. [35], who analysed the consequence of an isothermal annealing on the microstructure and mechanical behaviour of Al–Si12 parts manufactured by L-PBF. When the temperature was progressively increased from 473 K (200 °C) to 723 K (450 °C), the microstructure became coarser and silicon migrated into precipitates of increasing size. The yield strength decreased significantly, but the fracture strain increased by a factor of 5 [35].

Rao et al. [21] also reported that, for A357.0 parts produced by L-PBF, a rapid microstructure coarsening occurs during heat treatment

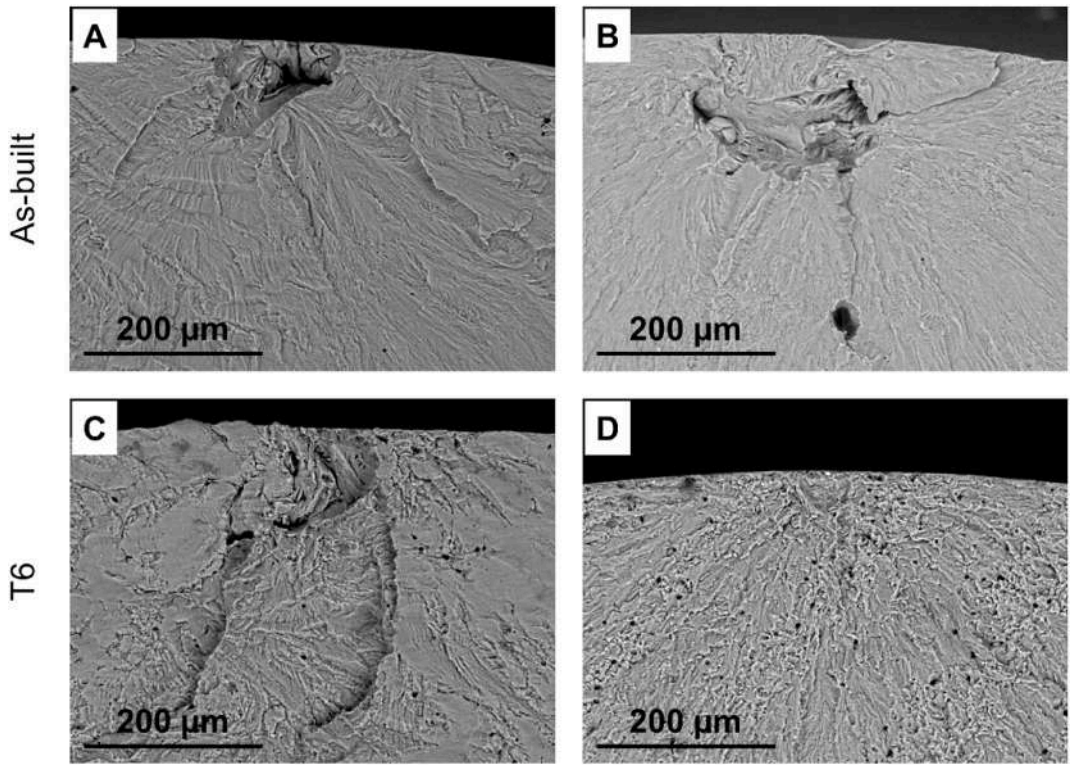

Fig. 6. Fracture surfaces of "average samples": first zone with triggering defect. A) XY-AB; B) Z-AB; C) XY-T6; D) Z-T6.

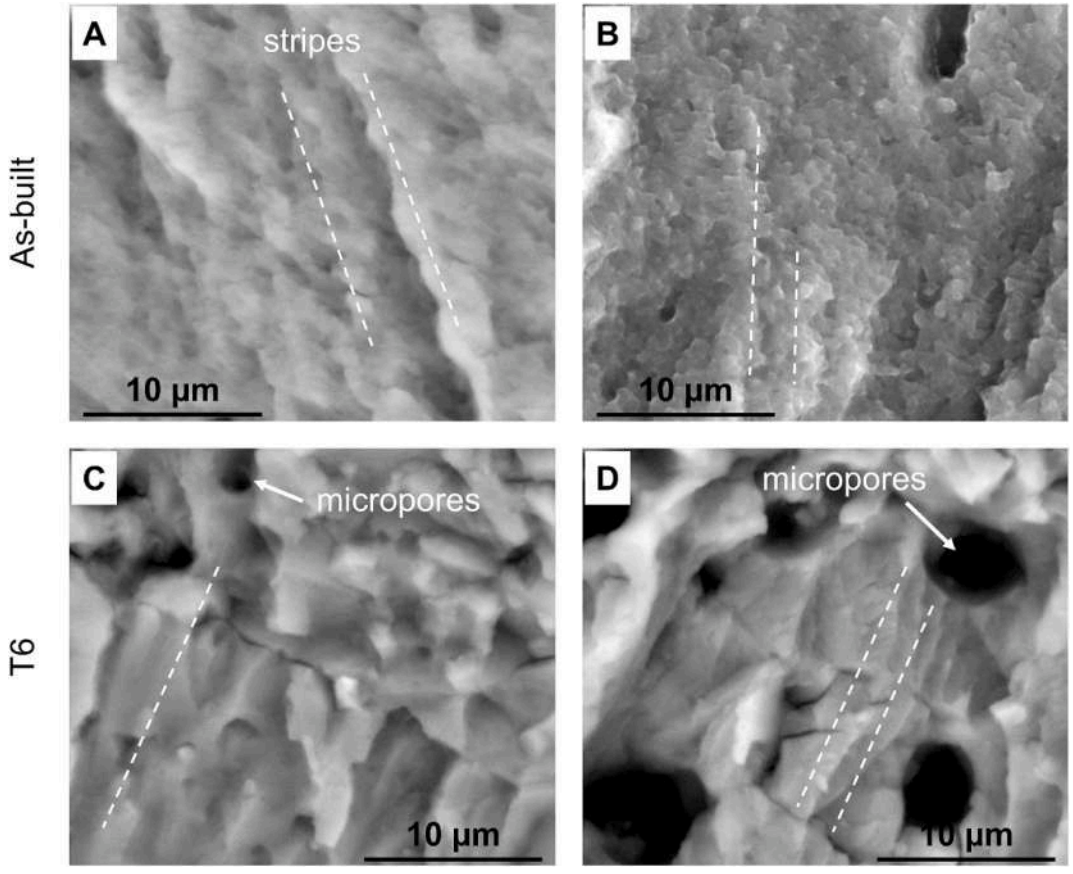

Fig. 7. Fracture surfaces of "average samples": second transition zone. A) XY-AB; B) Z-AB; C) XY-T6; D) Z-T6.

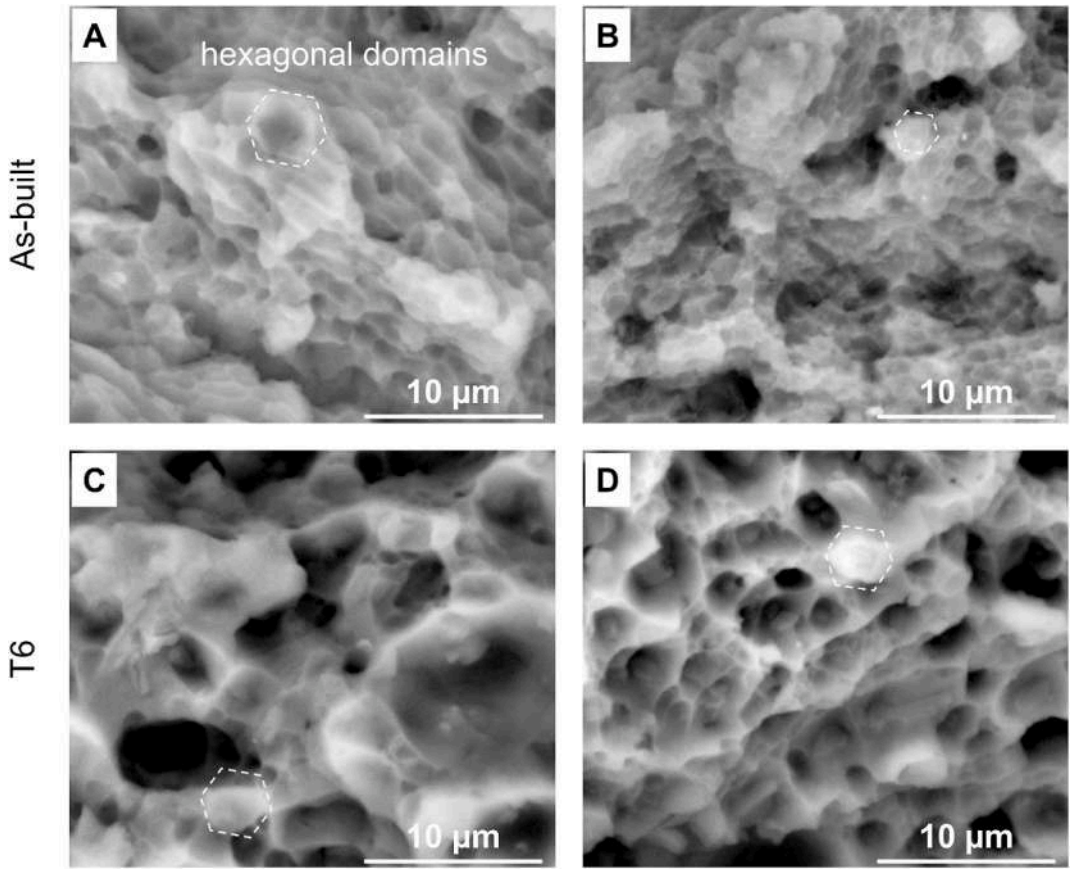

Fig. 8. Fracture surfaces of "average samples": third final zone. A) XY-AB; B) Z-AB; C) XY-T6; D) Z-T6.

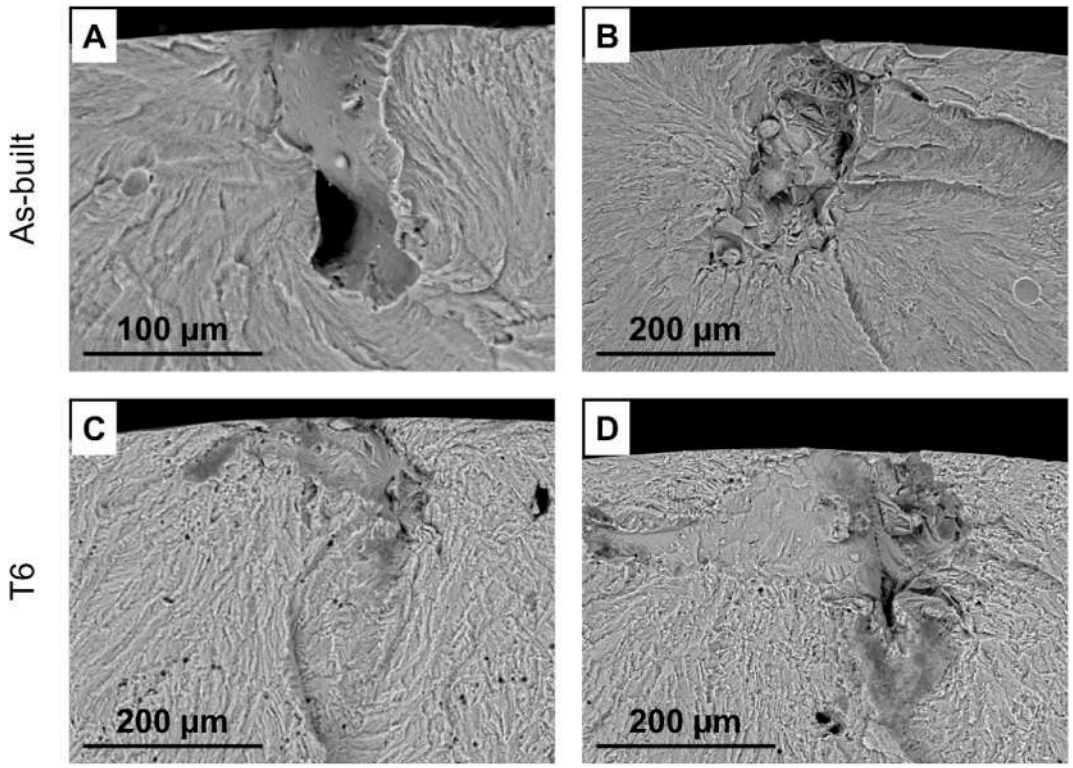

Fig. 9. Fracture surfaces of "early broken samples": first zone with triggering defect. A) XY-AB; B) Z-AB; C) XY-T6; D) Z-T6.

as the temperature approaches the eutectic point of 540 °C, with adverse effects on the mechanical performance.

In the present research, the results reported in Table 2 clearly show that the T6 treatment did not improve the average fatigue strength that was already high in the AB condition (typical values for additively manufactured aluminium-based parts can be found in Ref. [36]) and remained substantially unchanged after T6 treatment.

This is in contrast with the results presented by Aboulkhair et al. [32], who observed instead a significant improvement in fatigue strength after T6 treatment of AlSi10Mg parts processed under a baseplate pre-heating condition of 190 °C. The enhancement in fatigue performance was attributed to the combined action of various phenomena, including shape change of Si dendrites to spheroids that hinder crack initiation and propagation, randomization of crystallographic texture and consequent increase in ductility of the material.

Contrary to the results presented by Aboulkhair et al. [32], in the present contribution, as shown in Table 2, the fatigue strength was comparable before and after T6 treatment. The insensitivity of the fatigue strength to thermal treatment derives from the specific crack initiation mechanisms that are active in the L-PBF samples under investigation here, as proven by the SEM inspection of the fractured coupons. In fact, the SEM observation reveals that fracture is usually initiated by lack of fusion defects, which remain unchanged after T6 treatment. In more detail, as shown in Fig. 6, for all the "average samples" fracture is initiated by a lack of fusion defect that is located either on the lateral surface or just slightly below the surface. It is well known that pores close to the surface are detrimental to fatigue resistance [37]. The different depth and extension of the triggering defects are likely to cause uneven fatigue performance. For the XY specimens, the fracture surfaces attest that the interlayer bonding is so good that the layered structure is not visible. Based on the SEM inspection, no specific inhomogeneity or stratification can be detected in the Z direction. After the first initiation zone, the fracture surface changes to a second transition zone, with a typical striped morphology (Fig. 7), and then to a third final zone, with very fine hexagonal domains that are associated to the presence of silicon precipitates at the boundaries of a cellular microstructure (Fig. 8) [36].

In some "average samples" in their T6 conditions, the defect that acts as crack initiator is slightly smaller than in the as-built samples. In that case, a diffused microporosity can be observed on the rupture surface (Fig. 7C and D), with pores below 50 μm that can be ascribed to the T6 treatment. The presence of these pores in the T6 condition is consistent with the values for residual porosity already reported in Table 1. In fact, entrapped gas pores can expand during heat treatment [21].

"Early broken samples" are generally similar to the "average samples" discussed above, but lack of fusion defects are generally bigger or more superficial as exemplified in Fig. 9.

It can be concluded, therefore, that failure mechanisms are governed by occasional defects that may be built within the specimens but whose dimensions and occurrence are generally less critical than achieved by casting [38]. The latter is also consistent with the observation that the fatigue strength results obtained in the present research are higher than the typical values for cast parts. The ineffectiveness of the T6 heat treatment to improve the fatigue behaviour can be attributed to the predominance in crack initiation and propagation of microstructural defects that cannot be mitigated by thermal treatment, as also observed in the past for cast aluminium [38].

Although a direct comparison is not straightforward, since the samples were built with a diverse L-PBF machine and since different loading conditions were applied upon fatigue testing, in a previous contribution the average fatigue strength of A357.0 parts at 2×10^6 cycles with $R = 0$ was statistically determined to be 60 MPa, with a standard deviation of 5.3 MPa [36].

It is meaningful that a superior fatigue performance was measured for the A357.0 parts considered here. It may derive from the lower porosity and it certainly confirms that the performance of L-PBF parts is little repeatable across different machines and process parameters.

As to the effect of build orientation, anisotropic behaviour in metal parts fabricated by PBF is still the object of intensive research. Several researchers have reported that, under quasi-static tensile loads, horizontally fabricated parts achieve higher mechanical properties (including yield strength, ultimate tensile strength, elongation) with respect to vertically fabricated samples. This is the case, for example, of the A357.0 tensile samples processed by means of L-PBF and tested as-built and after thermal treatment by Yang et al. [22]. However, also opposite behaviour was described in the literature, where horizontally fabricated parts exhibited lower mechanical properties [39]. Prashanth et al. [35] controlled the texture of as-produced AlSi12 tensile specimens produced via L-PBF by changing the inclination angle between the loading direction and the build platform. As the inclination angle approached 90°, the texture progressively increased. Nonetheless, the effect of texture on the tensile strength was proven to be irrelevant, being the yield strength insensitive to the inclination angle [35]. Rao et al. [20] compared the behaviour of A357.0 parts obtained by L-PBF under optimized conditions to achieve maximum density. The tensile mechanical properties were markedly anisotropic, with poorer tensile properties observed for vertical test samples than for horizontal ones. In fact, along the build direction, the coarsened silicon cells that developed after processing led to intercellular failure for crack growth, which decreased the tensile properties [20]. However, pre-heating the build platform is known to minimize the anisotropy of the finished part [9]. The results in Table 2 confirm this effect, as the average fatigue strength was comparable for horizontal and vertical samples, before and after T6 treatment. XY direction shows a slight advantage in terms of standard deviation, which turns into a better repeatability.

4. Conclusions

A357.0 parts were produced by laser-based powder bed fusion (L-PBF) with an in-situ annealing treatment via baseplate pre-heating. The staircase method was applied to statistically assess the fatigue strength in the as-built condition and after T6 heat treatment. Samples parallel to the baseplate or parallel to the growth direction were tested separately and compared. The average fatigue strength at the given life time of 1×10^7 cycles was insensitive to the build direction as a result of baseplate pre-heating, which minimizes anisotropic effects, and was unaltered after T6 treatment. In fact, the fracture initiation was controlled by the presence of sub-surface lack of fusion defects, which remained unchanged after heat treatment. These outcomes prove therefore that the fatigue behaviour is controlled by defects and not by the generated microstructure or by the slight increase in porosity due to the T6. If the L-PBF processing parameters of aluminium-based alloys are optimized so as to minimize inherent defects, pre-heating the baseplate during fabrication is sufficient to eliminate the effects of anisotropy and to maximize the fatigue resistance in the as-built condition.

Data availability

The data that support the findings of this study are available [40].

CRediT authorship contribution statement

S. Defanti: Investigation, Data curation, Validation, Formal analysis, Writing - original draft, preparation. **E. Bassoli:** Conceptualization, Methodology, Writing - review & editing, Supevision, Funding acquisition.

Declaration of competing interest

The authors declare that they have no known competing financial interests or personal relationships that could have appeared to influence the work reported in this paper.

Acknowledgements

This project has received funding from the European Union's Horizon 2020 research and innovation program under grant agreement No 723699. The authors would like to acknowledge EOS Finland Oy for the production of the specimens and the technical support.

References

[1] A. Aversa, M. Lorusso, F. Trevisan, E. Ambrosio, F. Calignano, D. Manfredi, S. Biamino, P. Fino, M. Lombardi, M. Pavese, Effect of process and post-process conditions on the mechanical properties of an A357 alloy produced via laser powder bed fusion, Metals 7 (2017) 68, https://doi.org/10.3390/met7020068.
[2] P. Mercelis, J. Kruth, Residual stresses in selective laser sintering and selective laser melting, Rapid Prototyp. J. 12 (2006) 254–265, https://doi.org/10.1108/13552540610707013.
[3] T. Simson, A. Emmel, A. Dwars, J. Böhm, Residual stress measurements on AISI 316L samples manufactured by selective laser melting, Addit. Manuf. 17 (2017) 183–189, https://doi.org/10.1016/j.addma.2017.07.007.
[4] C. Li, J.F. Liu, X.Y. Fang, Y.B. Guo, Efficient predictive model of part distortion and residual stress in selective laser melting, Addit. Manuf. 17 (2017) 157–168, https://doi.org/10.1016/j.addma.2017.08.014.
[5] B. Ahmad, S.O. van der Veen, M.E. Fitzpatrick, H. Guo, Residual stress evaluation in selective-laser-melting additively manufactured titanium (Ti-6Al-4V) and inconel 718 using the contour method and numerical simulation, Addit. Manuf. 22 (2018) 571–582, https://doi.org/10.1016/j.addma.2018.06.002.
[6] Y. Liu, Y. Yang, D. Wang, A study on the residual stress during selective laser melting (SLM) of metallic powder, Int. J. Adv. Manuf. Technol. 87 (2016) 647–656, https://doi.org/10.1007/s00170-016-8466-y.
[7] C. Li, Z.Y. Liu, X.Y. Fang, Y.B. Guo, Residual stress in metal additive manufacturing, Procedia CIRP 71 (2018) 348–353, https://doi.org/10.1016/j.procir.2018.05.039.
[8] D. Buchbinder, W. Meiners, N. Pirch, K. Wissenbach, J. Schrage, Investigation on reducing distortion by preheating during manufacture of aluminum components using selective laser melting, J. Laser Appl. 26 (2014), https://doi.org/10.2351/1.4828755, 01–10.
[9] E. Brandl, U. Heckenberger, V. Holzinger, D. Buchbinder, Additive manufactured AlSi10Mg samples using Selective Laser Melting (SLM): microstructure, high cycle fatigue, and fracture behavior, Mater. Des. 34 (2012) 159–169, https://doi.org/10.1016/j.matdes.2011.07.067.
[10] A. Gatto, E. Bassoli, L. Denti, A. Sola, E. Tognoli, A. Comin, J.A. Porro, F. Cordovilla, I. Angulo, J.L. Ocaña, Effect of three different finishing processes on the surface morphology and fatigue life of A357.0 parts produced by laser-based powder bed fusion, Adv. Eng. Mater. 21 (2019) 1801357, https://doi.org/10.1002/adem.201801357.
[11] E. Atzeni, M. Barletta, F. Calignano, L. Iuliano, G. Rubino, V. Tagliaferri, Abrasive fluidized bed (AFB) finishing of AlSi10Mg substrates manufactured by direct metal laser sintering (DMLS), Addit. Manuf. 10 (2016) 15–23, https://doi.org/10.1016/j.addma.2016.01.005.
[12] A. Salmi, E. Atzeni, L. Iuliano, M. Galati, Experimental analysis of residual stresses on AlSi10Mg parts produced by means of selective laser melting (SLM), Procedia CIRP 62 (2017) 458–463, https://doi.org/10.1016/j.procir.2016.06.030.
[13] P. Edwards, M. Ramulu, Fatigue performance evaluation of selective laser melted Ti–6Al–4V, Mater. Sci. Eng. 598 (2014) 327–337, https://doi.org/10.1016/j.msea.2014.01.041.
[14] J.G. Kaufman, Understanding wroughtand cast AluminumAlloys designations, in: Introd. To Alum. Alloy. Tempers, ASM International, 2000, pp. 23–37, https://doi.org/10.1361/iaat2000p023.
[15] A. Saboori, M. Pavese, C. Badini, A.R. Eivani, Studying the age hardening kinetics of A357 aluminum alloys through the Johnson–Mehl–Avrami theory, Met. Powder Rep. 72 (2017) 420–424, https://doi.org/10.1016/j.mprp.2016.08.006.
[16] X. Yang, J. Zhu, Z. Nong, D. He, Z. Lai, Y. Liu, F. Liu, Prediction of mechanical properties of A357 alloy using artificial neural network, Trans. Nonferrous Metals Soc. China 23 (2013) 788–795, https://doi.org/10.1016/S1003-6326(13)62530-3.
[17] N.T. Aboulkhair, C. Tuck, I. Ashcroft, I. Maskery, N.M. Everitt, On the precipitation hardening of selective laser melted AlSi10Mg, Metall. Mater. Trans. 46 (2015) 3337–3341, https://doi.org/10.1007/s11661-015-2980-7.
[18] E. Girardin, G. Barucca, P. Mengucci, F. Fiori, E. Bassoli, A. Gatto, L. Iuliano, B. Rutkowski, Biomedical Co-Cr-Mo components produced by direct metal laser sintering, Mater. Today Proc. 3 (2016) 889–897, https://doi.org/10.1016/j.matpr.2016.02.022.
[19] F. Trevisan, F. Calignano, M. Lorusso, J. Pakkanen, E.P. Ambrosio, L. Mariangela, M. Pavese, D. Manfredi, P. Fino, Effects of heat treatments on A357 alloy produced by Selective Laser Melting, in: Eur. Congr. Exhib. Powder Metall., 2016, pp. 1–6.
[20] H. Rao, S. Giet, K. Yang, X. Wu, C.H.J. Davies, The influence of processing parameters on aluminium alloy A357 manufactured by Selective Laser Melting, Mater. Des. 109 (2016) 334–346, https://doi.org/10.1016/j.matdes.2016.07.009.
[21] J.H. Rao, P. Rometsch, X. Wu, C.H.J. Davies, The processing and heat treatment of selective laser melted Al-7Si-0.6Mg alloy, in: Addit. Manuf. Aerosp. Ind., Elsevier, 2019, pp. 143–161, https://doi.org/10.1016/B978-0-12-814062-8.00008-X.
[22] K.V. Yang, P. Rometsch, C.H.J.H.J. Davies, A. Huang, X. Wu, Effect of heat treatment on the microstructure and anisotropy in mechanical properties of A357 alloy produced by selective laser melting, Mater. Des. 154 (2018) 275–290, https://doi.org/10.1016/j.matdes.2018.05.026.
[23] A. Majeed, Y. Zhang, J. Lv, T. Peng, Z. Atta, A. Ahmed, Investigation of T4 and T6 heat treatment influences on relative density and porosity of AlSi10Mg alloy components manufactured by SLM, Comput. Ind. Eng. 139 (2020) 106194, https://doi.org/10.1016/j.cie.2019.106194.
[24] J.C. Pereira, E. Gil, L. Solaberrieta, M. San Sebastián, Y. Bilbao, P.P. Rodríguez, Comparison of AlSi7Mg0.6 alloy obtained by selective laser melting and investment casting processes: microstructure and mechanical properties in as-built/as-cast and heat-treated conditions, Mater. Sci. Eng. 778 (2020) 139124, https://doi.org/10.1016/j.msea.2020.139124.
[25] Uni En 3987:2010, Aerospace Series - Test Methods for Metallic Materials - Constant Amplitude Force-Controlled High Cycle Fatigue Testing, European Committee for Standardization, Brussels, Belgium, 2010.
[26] Iso 12107:2012, Fatigue Testing - Statistical Planning and Analysis of Data, International Organization for Standardization, Geneva, Switzerland, 2012.
[27] S. Romano, S. Beretta, A. Brandão, J. Gumpinger, T. Ghidini, HCF resistance of AlSi10Mg produced by SLM in relation to the presence of defects, Procedia Struct. Integr. 7 (2017) 101–108, https://doi.org/10.1016/j.prostr.2017.11.066.
[28] Astm E466-15, Standard Practice for Conductiong Force Controlled Constant Amplitude Axial Fatigue Tests of Metallic Materials, ASTM International, West Conshohocken, PA, 2015, https://doi.org/10.1520/E0466-15.
[29] American Society for Metals, ASM Handbook Volume 2: Properties and Selection: Nonferrous Alloys and Special-Purpose Materials, ASM International, 1990.
[30] Iso 6506-1:2014, Metallic Materials - Brinell Hardness Test - Part 1: Test Method, International Organization for Standardization, Geneva, Switzerland, 2014.
[31] A.B.B. Spierings, M. Schneider, R. Eggenberger, Comparison of density measurement techniques for additive manufactured metallic parts, Rapid Prototyp. J. 17 (2011) 380–386, https://doi.org/10.1108/13552541111156504.
[32] N.T. Aboulkhair, I. Maskery, C. Tuck, I. Ashcroft, N.M. Everitt, Improving the fatigue behaviour of a selectively laser melted aluminium alloy: influence of heat treatment and surface quality, Mater. Des. 104 (2016) 174–182, https://doi.org/10.1016/j.matdes.2016.05.041.
[33] F. Du, C. Li, Z. Mi, Y. Shen, R. Huang, X. Han, Y. Dong, J. Xu, Anti-wear property of aluminum–silicon alloy treated by chemical etching, Mechanical Honing and Laser Finishing, Materials (Basel) 12 (2019) 1273, https://doi.org/10.3390/ma12081273.
[34] D. Buchbinder, W. Meiners, K. Wissenbach, R. Poprawe, Selective laser melting of aluminum die-cast alloy—correlations between process parameters, solidification conditions, and resulting mechanical properties, J. Laser Appl. 27 (2015) S29205, https://doi.org/10.2351/1.4906389.
[35] K.G. Prashanth, S. Scudino, H.J. Klauss, K.B. Surreddi, L. Löber, Z. Wang, A. K. Chaubey, U. Kühn, J. Eckert, Microstructure and mechanical properties of Al–12Si produced by selective laser melting: effect of heat treatment, Mater. Sci. Eng. 590 (2014) 153–160, https://doi.org/10.1016/j.msea.2013.10.023.
[36] E. Bassoli, L. Denti, A. Comin, A. Sola, E. Tognoli, Fatigue behavior of as-built L-PBF A357.0 parts, Metals 8 (2018) 634, https://doi.org/10.3390/met8080634.
[37] M. Thöne, S. Leuders, A. Riemer, T. Tröster, H.A. Richard, Influence of heat-treatment on selective laser melting products, in: Solid Free. Fabr. Proceedings, Proc. Annu. Int. Solid Free, Fabr. Symp., 2012, pp. 492–498.
[38] J.M. Boileau, J.E. Allison, The effect of solidification time and heat treatment on the fatigue properties of a cast 319 aluminum alloy, Metall. Mater. Trans. 34 (2003) 1807–1820, https://doi.org/10.1007/s11661-003-0147-4.
[39] C. Qiu, N.J.E.E. Adkins, M.M. Attallah, Microstructure and tensile properties of selectively laser-melted and of HIPed laser-melted Ti–6Al–4V, Mater. Sci. Eng. 578 (2013) 230–239, https://doi.org/10.1016/j.msea.2013.04.099.
[40] E. Bassoli, S. Defanti, A357.0 Fatigue Test, vol. 1, Mendeley Data, 2020. https://doi.org/10.17632/3rb4rdhrhb.1.